Nanografting for Surface Physical Chemistry

Maozi Liu,[1] Nabil A. Amro,[2] and Gang-yu Liu[3]

[1]Agilent Technologies, Inc., Santa Clara, California 95051;
email: maozi_liu@agilent.com

[2]NanoInk, Inc., Skokie, Illinois 60077; email: namro@nanoink.net

[3]Department of Chemistry, University of California, Davis, California 95616;
email: liu@chem.ucdavis.edu

Annu. Rev. Phys. Chem. 2008. 59:367–86

First published online as a Review in Advance on November 19, 2007

The *Annual Review of Physical Chemistry* is online at http://physchem.annualreviews.org

This article's doi:
10.1146/annurev.physchem.58.032806.104542

0066-426X/08/0505-0367$20.00

Key Words

size-dependent property, spatially confined surface chemistry, phase segregation, scanning probe lithography

Abstract

This article reveals the enabling aspects of nanografting (an atomic force microscopy–based lithography technique) in surface physical chemistry. First, we characterize self-assembled monolayers and multilayers using nanografting to place unknown molecules into a matrix with known structure or vice versa. The availability of an internal standard in situ allows the unknown structures to be imaged and quantified. The same approaches are applied to reveal the orientation and packing of biomolecules (ligands, DNA, and proteins) upon immobilization on surfaces. Second, nanografting enables systematic investigations of size-dependent mechanics at the nanometer scale by producing a series of designed nanostructures and measuring their Young's modulus in situ. Third, one can investigate systematically the influence of ligand local structure on biorecognition and protein immobilization by precisely engineering ligand nanostructures. Finally, we also demonstrate the regulation of the surface reaction mechanism, kinetics, and products via nanografting.

INTRODUCTION

AFM: atomic force microscopy

SAM: self-assembled monolayer

Nanostructures: assemblies of atoms, molecules, or ions with an overall dimension of less than 100 nm

Nanografting was reported in 1997 using combined atomic force microscopy (AFM) with the surface chemistry of thiol adsorption on gold surfaces (1). The procedure of nanografting is relatively simple, starting from imaging (under a small force) an alkanethiol self-assembled monolayer (SAM) in a liquid medium containing a different kind of thiol (**Figure 1*a***). As a higher force is applied during the scanning, the matrix thiol molecules are removed by the tip and transported into the solvent. Thiol molecules contained in the solution immediately adsorb onto the freshly exposed gold area following the scanning track of the atomic force microscope tip to form designed nanostructures. The produced nanopatterns can then be characterized in situ by the same atomic force microscope tip at a reduced force.

Since its invention, researchers have reported much improvement and technological extensions of nanografting. For example, reversal nanografting was developed to improve the throughput (2). In this process, functional molecules were first deposited on surfaces, and then inert components were placed, using nanografting, to separate the functional molecules into arrays of designed nanostructures. **Figure 1*b*** shows an

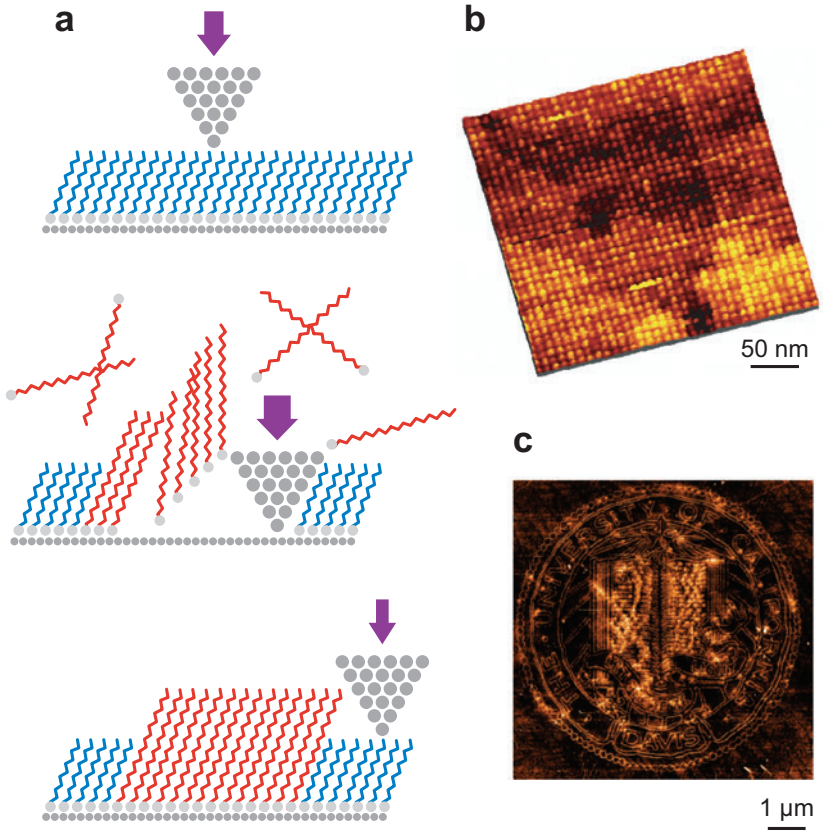

Figure 1

(*a*) Schematic showing the process of nanografting. (*b*) A 33 × 33 array of nanostructures of biotin-terminated thiols inlaid in hexanethiol matrix, produced in an ethanol medium using nanografting. (*c*) An 8 μm × 8 μm lateral force image of the University of California at Davis seal produced by nanografting.

example in which a 33 × 33 array of biotin-terminated thiols was produced on gold. Each element has a size of 5.2 × 5.2 nm^2 with great uniformity. Nanopen reader and writer extends nanografting into ambient or nonreactive media (3). In nanopen reader and writer, reactants are predeposited onto an atomic force microscope probe. The probe can then perform AFM imaging under low load and deposit the desired materials under high force on a gold surface by replacing the resist molecules. Software and digitization in scanning probe lithography also significantly improved to enable automated nanolithography for the high-throughput production of complex nanostructures and arrays (4). **Figure 1*c*** illustrates a revealing example in which the University of California at Davis's seal is fabricated by nanografting an aldehyde terminated thiol into a decanethiol SAM. The process took 10 min to complete with the finest width of 10 nm. The automated nanografting may be utilized in conjunction with multiple atomic force microscope tips in a one- or two-dimensional format for the parallel fabrication of nanopatterns. Furthermore, researchers have also reported modified nanografting by regulating local interactions, such as adsorbates on silica or silicon surfaces (5), tapping mode nanografting (6), and scanning tunneling microscopy–based nanografting (7).

Resist: a thin film coating on surfaces that serves as precursor and sacrificial layer for lithography

Ligand: a molecule able to bind to and form a complex with a biomolecule; an effector molecule binding to a site on a target protein by intermolecular forces

Molecular resolution: the capability of distinguishing between two separate but adjacent molecules

Similar to many scanning probe lithography techniques—such as scanning tunneling microscopy–based lithography (8–10), dip-pen nanolithography (11, 12), local oxidation nanolithography (13, 14), and local chemical or electrochemical lithography (15)—nanografting has many advantages in the context of potential applications in material science and the nanotechnology industry. For instance, the spatial resolution is high; thus the production and characterization of sub-100-nm structures become feasible. Nanografting also shows great promise in materials science by producing various functional nanostructures, including -OH, -COOH, -CHO, $-NH_2$, -NHS, biotin, $-CF_3$, carbohydrate, and nucleotides (16–20). One can construct three-dimensional nanostructures using pattern transfer by further surface reactions (21, 22). Moreover, the versatility of nanografting has been demonstrated by the creation of nanostructures of large molecules and biological molecules, such as nanoparticles of metals (23, 24), DNA (25, 26), ligands (20), and proteins (18, 27). Finally, many researchers and laboratories that have AFM capabilities favor nanografting for its simplicity.

Four unique aspects of nanografting make it a new and powerful tool in surface physical chemistry. First, by not requiring any tip modification and eliminating surface diffusion using a SAM as a resist, nanografting harnesses the highest spatial resolution AFM can offer both in nanostructure production and in characterization (28). Second, nanografting can work in versatile chemical environments (e.g., wet chemistry), which enables direct mimicking and monitoring of real-surface reactions in situ, in real time, and with molecular resolution (29). Third, as discussed below, nanografting is an active tool for regulating the reaction mechanism, kinetics, and products. Fourth, multiplexing is enabled within one experiment by producing multicomponent nanostructures and then introducing designed reactants while monitoring the outcome in situ.

As previous reviews have discussed eloquently the potential of nanografting in material assembly, molecular electronics, and bioresearch (13, 29), this article focuses

on the enabling aspects of nanografting in surface physical chemistry. We discuss four fundamental scientific inquiries that are otherwise difficult to probe without nanografting: (*a*) surface structural characterization at the molecular level; (*b*) the size-dependent Young's modulus of monolayer materials; (*c*) the size and geometry dependence of protein immobilization and protein-ligand reactions; and (*d*) the regulation of the surface reaction mechanism, kinetics, and local structures.

SURFACE STRUTURAL CHARACTERIZATION USING NANOGRAFTING

Researchers have widely used AFM to visualize surface morphology and structure, especially for nonconductive materials, because of its high spatial resolution and ability to image a wide range of systems. AFM imaging has provided important and new structural information, such as local domains, phase segregations, defects, and short- and long-range order or periodicity (30–32). Although conventional AFM imaging provides a means for visualizing surface morphology, defects, and order and for quantifying surface roughness, it is difficult to extract information about molecular conformation, especially in the case of large molecules, such as long-chain organic molecules, polymers, and biomolecules. Nanografting, conversely, provides a powerful complement to conventional AFM imaging by determining the molecular conformation on surfaces using an internal reference, such as a resist or a matrix with well-known three-dimensional structures (e.g., alkanethiol SAMs). The height and lateral structure of the newly grafted molecules can thus be accurately measured, with the precision of a fraction of a nanometer, by direct comparison with the matrix molecules. Similarly, one may take a reverse approach in which a known alkanethiol SAM is nanografted in the films, whose structures can then be determined. The availability of an internal standard in situ allows the unknown structures to be imaged and quantified with high resolution.

Nanografting for the Structural Characterization of Self-Assembled Monolayers

SAMs with a wide variety of thiolated molecules have been characterized using nanografting. The simplest example is alkanethiols in which decanethiol SAMs (C_{10}) are used as the matrix/internal standard (**Figure 2**). Within the monolayers, decanethiols form close-packed domains with a commensurate ($\sqrt{3} \times \sqrt{3}$)R30° structure with respect to the Au(111) surface (see **Figure 2*d***) (33, 34). The molecules adopt an all-*trans* configuration, with a tilt angle of 30° from the surface normal. In addition, the zigzag planes of the chains may exhibit up to four twist angles, yielding various c($4\sqrt{3} \times 2\sqrt{3}$)R30° super lattices. With the assumption that the structure of octadecanethiols (C_{18}) was unknown, we nanografted the C_{18} molecules into the C_{10} matrix. The periodicity of C_{18} is the same as the surrounding C_{10} (i.e., a two-dimensional close-packed structure with a lattice constant of 0.50 nm) (**Figure 2*c***). The Au(111) lattice can be visualized during the nanoshaving step (**Figure 1*a***), enabling the determination of commensurateness of the thiol adsorbates. The height

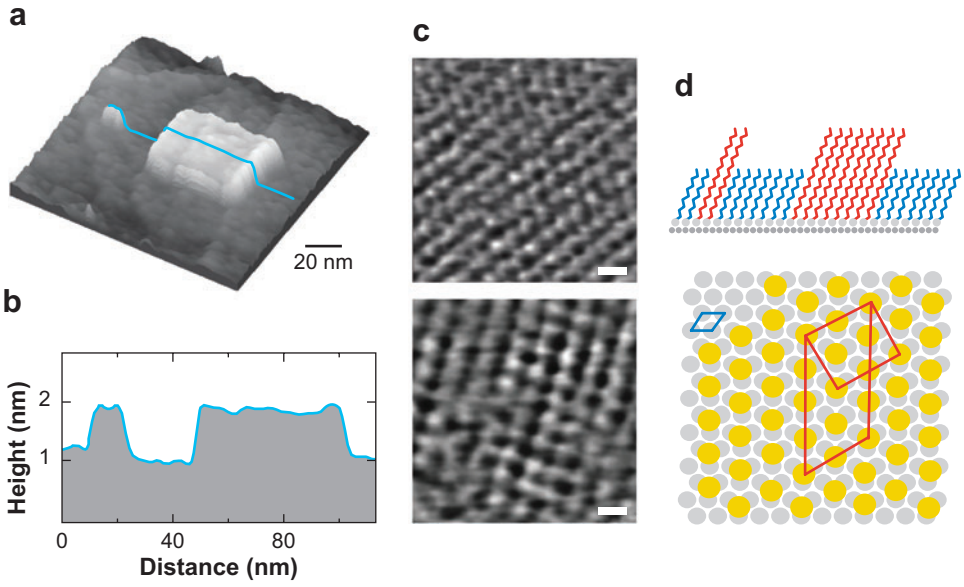

Figure 2

(*a*) Fabrication of two C_{18} nanoislands (2×4 and 50×50 nm^2) inlaid in the decanethiol matrix using nanografting. As shown in the cursor profile in panel *b*, the C_{18} island is 0.88 nm higher than the surrounding self-assembled monolayer (SAM). (*c*) Zoom-in scans reveal the closely packed structure of SAMs in the nanostructures (*top panel*) and matrix (*bottom panel*). Scale bar in **Figure 2*c*** is 0.5 nm. (*d*) Schematic diagram illustrating the structure of C_{18} SAM. (*Top panel*) The zigzag lines represent the hydrocarbon chains, with C_{18} shown in red and C_{10} shown in blue. (*Bottom panel*) The gray circles represent the gold atoms, and yellow dots represent sulfur head groups.

difference between C_{18} and C_{10} measured 0.88 ± 0.02 nm (**Figure 2*b***). Therefore, all C_{18} molecules adopt an all-*trans* configuration, with the chains tilted 30° from the surface normal (28, 29).

SAMs with nonalkane chains, such as arenethiols, have also been characterized using nanografting (35). The side-by-side comparison of arenethiol and alkanethiol SAMs is accomplished by grafting nanopatterns of alkanethiols within the matrix of arenethiol SAM or vice versa. Upon nanografting of 4-[4′(phenylethynyl)-phenylethynyl]-benzenethiols (PPBT) into a C_{10} matrix, the arenethiols are measured to be 7.6 ± 1.0 Å higher than the surrounding decanethiol matrix. Therefore, unlike alkanethiol SAMs in which molecules tilt 30° from the surface normal, arenethiol molecules are attached perpendicular to the surface. This conclusion is further confirmed by the nanografting of docosanethiol inlaid in a PPBT SAM, in which the alkanethiols are 6.5 ± 0.8 Å taller than the surrounding arenethiols. Both experiments validate the upright conformation of arenethiols within 5° accuracy.

Figure 3 provides another example in which the structure of SAMs with complex chain and termini is characterized (20). Using nanografting, we produced

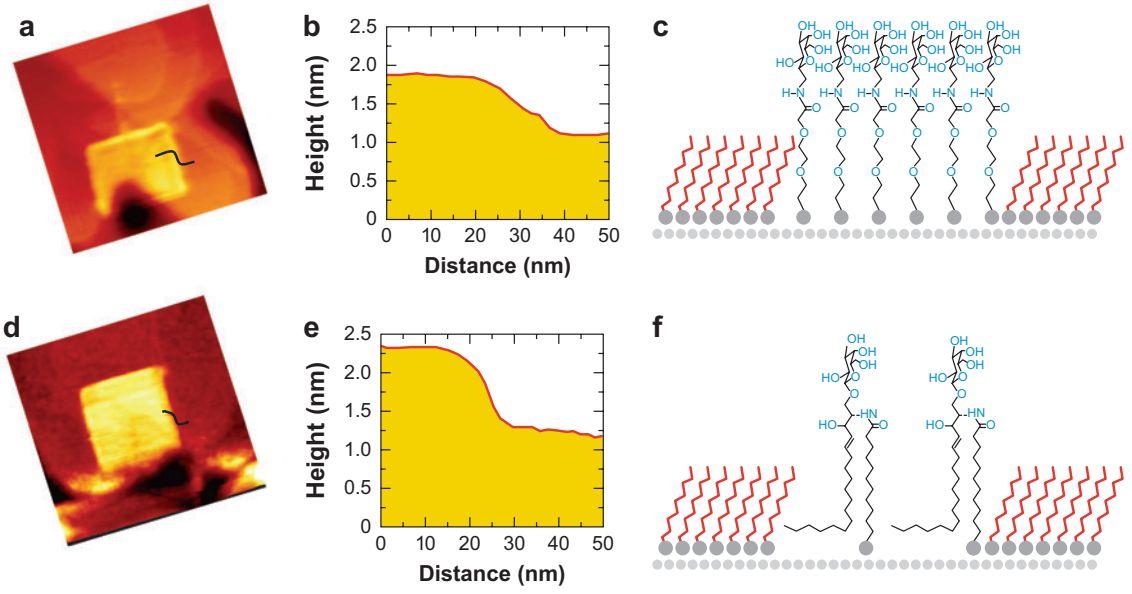

Figure 3

(*a*) A 300 nm × 300 nm atomic force microscopy (AFM) topographic image including a 130 nm × 110 nm rectangle of ligand Gal in a C_8 matrix self-assembled monolayer (SAM). (*b*) Cursor profile corresponding to the line in panel *a*. (*c*) Side view of Gal molecules in the pattern. (*d*) A 400 nm × 400 nm AFM topographic image including a 150 nm × 150 nm square of ligand GalCer in a C_{10} matrix SAM. (*e*) Cursor profile corresponding to the line in panel *d*. (*f*) Side view of the GalCer molecules in the pattern.

nanostructures of carbohydrate ligands, 2-[2(2-mercaptoethoxy)ethoxyl]-*N*-(galactopyranosyl-2′-methyl)acetamide (Gal) and β-D-galactopyranosyl-2S,3R,4E-3-hydroxy-2-*N*-(11-mercapto-undecanoic acid)-sphingenine (GalCer). **Figure 3** shows two nanostructures, a 130 nm × 110 nm ligand Gal pattern inlaid in a C_8 SAM (**Figure 3*a***), and a 150 nm × 150 nm GalCer-terminated thiol inlaid in a C_{10} SAM (**Figure 3*d***). The apparent height of the two nanostructures measured from cursor profiles (**Figure 3*b*,*e***) is 0.75 and 1.15 nm above the surrounding SAM, respectively. In contrast to alkane chains, which adopt a 30° tilt with respect to the surface normal, these apparent heights of Gal- and GalCer-terminated thiols suggest an upright configuration, as schematically shown in **Figure 3*c*,*f***. The configuration difference between alkanethiols and thiolated carbohydrate ligands in SAMs likely results from the intermolecular interactions. As shown in **Figure 3*c***, thiolated Gal molecules incorporate an ethylene glycol backbone with a bulky terminal, whereas thiolated GalCer (**Figure 3*f***) has two chains (one thiol head group and another just hydrocarbon with six carbon atoms more than the thiol chain). These molecular differences between alkanethiols and carbohydrate ligands impact the interchain interactions, and thus their final configurations within SAMs. Molecules within the nanostructure are closely packed, as evidenced by the small deformation under tip pressure.

Nanografting for Determining the Orientation and Packing of Biomolecules on Surfaces

Single-strand DNA or oligonucleotide molecules are routinely immobilized on surfaces as the initial step for constructing sensors, a solid-state synthesis, or a bioassay. The orientation and packing of the molecules impact the subsequent hybridization reactions and device performance. Nanografting offers a means to characterize the orientation and packing of DNA or oligonucleotides (25). Proof of concept has been demonstrated using two single-stranded oligomolecules, 5′-HS-$(CH_2)_6$CTAGCTCTAAT-CTGCTAG-3′ (here referred to as oligo 1) and 5′-HS-$(CH_2)_6$AGAAGGCCTAGA-3′ (here referred to as oligo 2) (25). On grafting a 115 × 135 nm^2 nanopattern of oligo 1 within a C_6 matrix, we measured the pattern to be 6.3–8.3 nm in height. A molecular model of oligo 1 yields a length of 8.4 nm in a fully stretched conformation. By comparison to the molecular model, one can conclude that oligo 1 is almost fully stretched. Similar results were attained for oligo 2, in which a 190 × 255 nm^2 pattern has an apparent height of 5.0–6.0 nm, by comparison with matrix C_{10} SAM.

The orientation and packing of proteins after immobilization on surfaces represent another class of important biomaterials that can benefit from in situ and high-resolution structural characterization. **Figure 4** shows an example in which lysozyme (LYZ) molecules were immobilized onto nanostructures of carboxyl termini (18). The high selectivity observed at pH 7 results mostly from electrostatic interactions between the LYZ molecules and the carboxylate-terminated nanopatterns. Three LYZ molecules are positioned along the 10 × 150 nm^2 nanoline, whereas eight protein particles are confined within the 100 × 150 nm^2 nanorectangle. The corresponding combined cursor profiles in **Figure 4*c*** reveal that the immobilized protein molecules

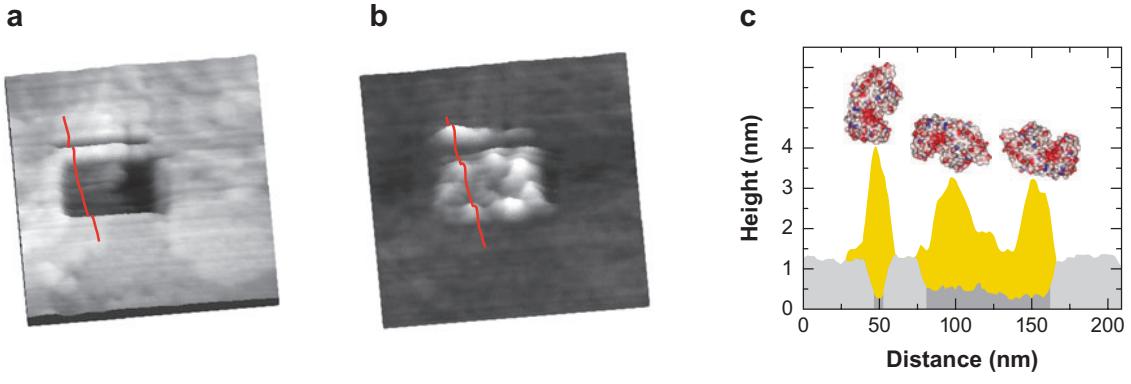

Figure 4

(*a*) A 10 nm × 150 nm line and a 100 nm × 150 nm rectangle of $HS(CH_2)_2COOH$ produced in C_{10} using nanografting. (*b*) The same area after introducing a lysozyme solution. (*c*) A combined cursor profile as indicated in panels *a* and *b*. Black and shaded areas represent the matrix and patterned self-assembled monolayer regions, respectively, whereas the yellow region corresponds to adsorbed protein molecules.

exhibit two different heights: 4.1 nm and 3.0 nm. The physical interactions are not specific; therefore, various orientations with respect to the surface are observed for the adsorbed proteins. Because LYZ molecules are ellipsoidal with the approximate dimensions $4.5 \times 3.0 \times 3.0\ nm^3$ from X-ray crystallographic studies, the observed heights (4.1 nm and 3.0 nm) correspond to the side-on and end-on orientations of LYZ, respectively (18).

When bioengineered with a chemical linkage (a cysteine at a specific site), proteins may be directly nanografted on solid support without introducing an extra linker. This site-specific modification will anchor the protein molecules in an appropriate matrix while preserving as best as possible the necessary function with a predictable adsorption and orientation to the surface. Using this approach, researchers patterned a 78-amino-acid iron(II) complex $[Fe(\alpha pV_aL_d\text{-}C26)_3]^{2+}$ via nanografting into a C_{18} SAM (36). The average value of the height difference is 3.1 nm between the protein and the matrix, giving a measured height for the proteins of 5.3 nm. This measurement compares well with the height of 5.2 nm predicted from molecular models (36).

Nanografting for Monitoring Structural Evolution

Investigators have also monitored the multilayer growth process using nanografting. Self-assembled multilayers of 4,4′-dimercaptobiphenyl (DMBP) may be formed by Cu(II)-catalyzed oxidation. The aromatic chains are known to stand upright; however, it was not completely clear if copper only acts as a catalyst or if it becomes part of the multilayer (37). Using nanografting, we produced a nanopattern of dodecanethiol in the monolayer of DMBP. This alkanethiol exhibits a height of 0.50 ± 0.18 nm, which is taller than the DMBP matrix monolayer. Because the known height of dodecanethiol is 1.54 nm, comparison gives the height of the DMBP monolayer as 1.04 ± 0.18 nm. On forming a second layer, the matrix became 0.67 nm taller than the dodecanethiol nanostructure. In another words, the thickness of the bilayer is 2.21 ± 0.25 nm. This height is consistent with the disulfide linkage between the first and second layer, but not consistent with the model of S-Cu-S sandwich formation. The addition of the third layer yielded the thickness of 3.36 ± 0.30 nm, which further verifies the formation of a disulfide linkage between layers (37).

Nanografting was also utilized to reveal the function of water in model membrane systems (38). First, the researchers produced a 100 nm × 100 nm–sized nanopatch of C_{18} in a SAM of hydroxyl-terminated alkanethiols, $HS(CH_2)_{11}OH$ ($C_{11}OH$) on Au(111), to roughly mimic the membranes' hydrophobic chains and polar head groups. They used contact-mode AFM to study the compressibility of these SAMs in the presence of 2-butanol. On changing the solvent to water, the mechanical resistance of the $C_{11}OH$ SAM became much higher than in 2-butanol. Because the compressibility of a hydrophobic C_{18} patch is not expected to change significantly from water to 2-butanol, it provides an ideal internal reference for the structure as well as mechanical resistance. This result is explained by molecular dynamics simulations in which water molecules can mediate the interaction between the OH head groups, relaxing the surface strain present in the case of 2-butanol and allowing the SAM hydrocarbon chains to form a more ordered crystal. If this were the case, it

would imply that the stabilizing action of water for biological membranes has a double nature.

Protein packing on surfaces has also been investigated using nanografting as a function of environmental pH (22). Bovine carbonic anhydrase (II) (CA) was immobilized onto charged nanopatches [6-mercaptohexan-1-ol (MCH), *N*-(6 mercapto) hexyl pyridinium bromide, and 3-mercaptopropionic acid] within a hexa(ethylene glycol)-terminated SAM. At pH 4.5, CA was immobilized onto both the negatively and positively charged patches. A careful analysis of line scan profiles reveals that the protein layer is not uniform, with the main part of the protein layer approximately 4–5 nm thick with domains up to 13 nm high (approximately three protein layers), suggesting that some CA molecules have aggregated at this pH. At pH 5, the protein-layer thickness decreased to approximately 4 nm (monolayer) on both negatively and positively charged surfaces. At pH 5.5 and 7.2, little CA was immobilized onto the positively charged nanopatch, but there was still complete coverage at the negatively charged surface. At pH 5.0 and 5.5, there was much less aggregation.

SIZE-DEPENDENT YOUNG'S MODULUS OF ORGANIC THIN FILMS

The development of the next generation of devices, chips, and micro- and nano-electromechanical systems demands advances in nanoscience and nanoengineering (39–41). The determination of the mechanical properties of nanostructures has received increasing attention lately owing to the rapid development of nanotechnology and the successful fabrication of many nanodevices and components. The measurement of local hardness, elasticity, and shear modulus of materials at the nanometer scale, however, is fraught with both theoretical and experimental challenges.

Nanografting enables one to address this challenge by producing nanostructures with designed size and geometry. These nanostructures are characterized using the same atomic force microscope tip, followed by force modulation spectroscopy and microscopy measurements (19). In force modulation, the sample is modulated at a designed frequency while the atomic force microscope probe remains in contact with the surface at a specified imaging force. The response amplitude and phase are acquired at the same time as the topographic image, from which one can determine the resonance frequency and viscoelastic behavior of each nanostructure or domain. To extract Young's modulus, investigators reported two methods: (*a*) calculating *E* from the amplitude and phase (42) and (*b*) calculating *E* from the resonance frequencies for the tip-surface contact (43–45).

Figure 5 shows the size-dependent mechanics of C_{18} SAM. First, C_{18} nanostructures are fabricated into a C_{10} matrix using nanografting with the designed size ranging from 20 nm to 200 nm in the lateral dimension (45). Force modulation spectra are then acquired, in which smaller nanostructures appear softer than larger ones as the resonance occurs at lower frequencies. The apparent Young's modulus decreases nonlinearly with the decreasing size of these nanostructures (45). At nanometer length scales, there are no longer sufficient neighbors to react to the applied pressure with the same behavior as a bulk film. This results in a decrease of the observed Young's

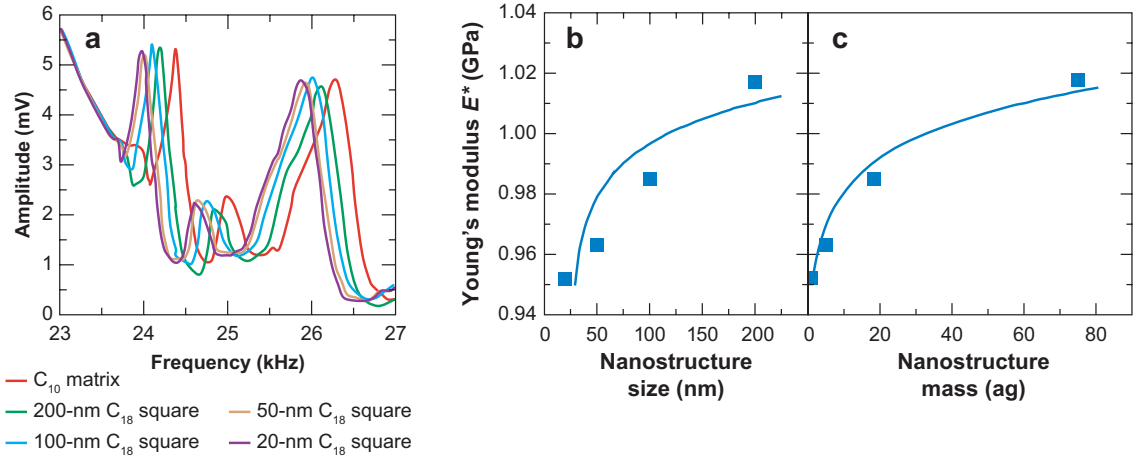

Figure 5

The spectra shown in panel *a* indicate a downshift of resonance with respect to the size. The Young's modulus of the structures is plotted against the size of the nanostructure in panel *b* and the mass of the nanostructure in panel *c*.

modulus. The systematic study using nanografting presents conclusive evidence of the size dependence of elasticity in the nanoregime. One may apply the approach utilized to study the size-dependence behavior of various materials and other mechanical properties.

IMPACT OF LOCAL LIGAND STRUCTURES ON BIOCHEMICAL REACTIONS

Extensive studies have revealed that human immunodeficiency virus type 1 (HIV-1) gains entry into host cells through the binding of its viral envelope protein gp120 with cellular receptors, such as CD4 or GalCer for CD4-negative cells (46). X-ray diffraction and electron microscopy investigations suggest that these membrane proteins present at the surface of HIV as trimers (47). The trimeric structures are likely to remain during the initial infection process (i.e., gp120 and cell-receptor binding are trivalent in nature). The V3 loop of gp120, which is the likely binding site for the T cell receptors, faces the trimer axis, with a separation ranging from 1.3 nm to 9.4 nm. Therefore, optimizing ligand nanostructures could offer an attractive mimetic for the initial viral binding (20).

Using nanografting, we produced a series of nanostructures (arrays of dots, lines, and cross-lines) of HIV binding ligands (20). **Figure 6*a–d*** shows four representative designs of nanostructures of GalCer termini and their potency in attracting gp120. For the nanostructure shown in **Figure 6*a***, few immobilized proteins are visible. The lack of protein adsorption is attributed to steric hindrance because the closely packed neighbor molecules make the GalCer difficult to access by the V3 loop of rgp120. In contrast, other designs exhibit potent binding to gp120. As visualized in

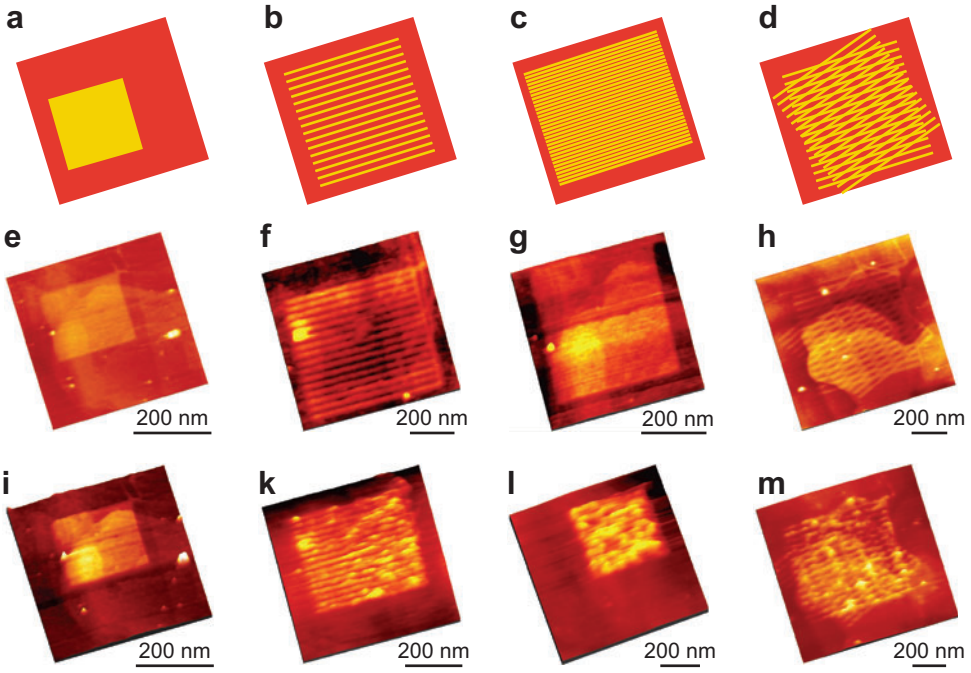

Figure 6

(*a–d*) Four designs of GalCer nanostructures. (*e*) Atomic force microscopy (AFM) topograph of a 200 nm × 200 nm GalCer square pattern produced using nanografting. (*f*) AFM topograph of an array of 16 lines covering a 400 nm × 400 nm area. (*g*) An array of 32 lines covering a 400 nm × 400 nm area. (*h*) AFM topograph of two arrays of lines crossing in space. Each line array contains 16 lines homogeneously distributed within 600 nm × 600 nm areas, and the two arrays are rotated 30° with respect to each other. (*i–m*) Same area as shown in panels *e* through *h* after a 60-min immersion in a 25 μg ml^{-1} rgp120 solution.

Figure 6*m*, most of the bright features are located in the crossed points, at which trivalent binding is favored.

The optimal size and geometry were determined using arrays with various dimensions, such as changing the angle of the cross-lines from 15° to 90° and changing the space of line arrays from 3 to 10 nm (20). Those systematic studies allow the determination of the optimal separation: 4.8 nm among nearest-neighbor GalCer is recommended for the design ligand mimetics.

We took a similar approach to investigate size-dependent biorecognition between biotin and antibiotin IgG, in which three arrays of biotin nanostructures were produced (2). IgG molecules prefer those structures in which biotin ligands are available at approximately 14.5-nm separation, confirming the bivalent and specific nature of the Fab domains with the underneath biotin termini. Protein immobilization via covalent binding to aldehyde groups has also been investigated. This protein attachment protocol occurs with at least two binding sites because the immobilization depends sensitively on the size and separation of the CHO domains. The multianchored

attachment is realized by the availability of lysine residues (83 per IgG and 9 per LYZ), and the matching aldehyde termini underneath, engineered using nanografting (2).

REGULATION OF SURFACE REACTION PATHWAYS, KINETICS, AND PRODUCTS

The self-assembly of thiols on gold provides a good example to illustrate the concept of regulating surface reactions using nanografting because the reaction kinetics and mechanism are relatively well-known. The significance of SAMs is clearly demonstrated from the large number of publications (~700) focusing on them since their discovery (48). **Figure 7*a*** illustrates the reaction mechanism or pathway of self-assembly. It is known from SPM (28, 33) and diffraction studies (49) that unconstrained self-assembly includes two main steps. Molecules initially attach to gold with the chains parallel to the surface, with a reaction intermediate known as the lying-down phase (**Figure 7*a***). As the reaction proceeds, thiols stand up and eventually form a complete layer, a result of collision and lateral pressure. In dilute solutions,

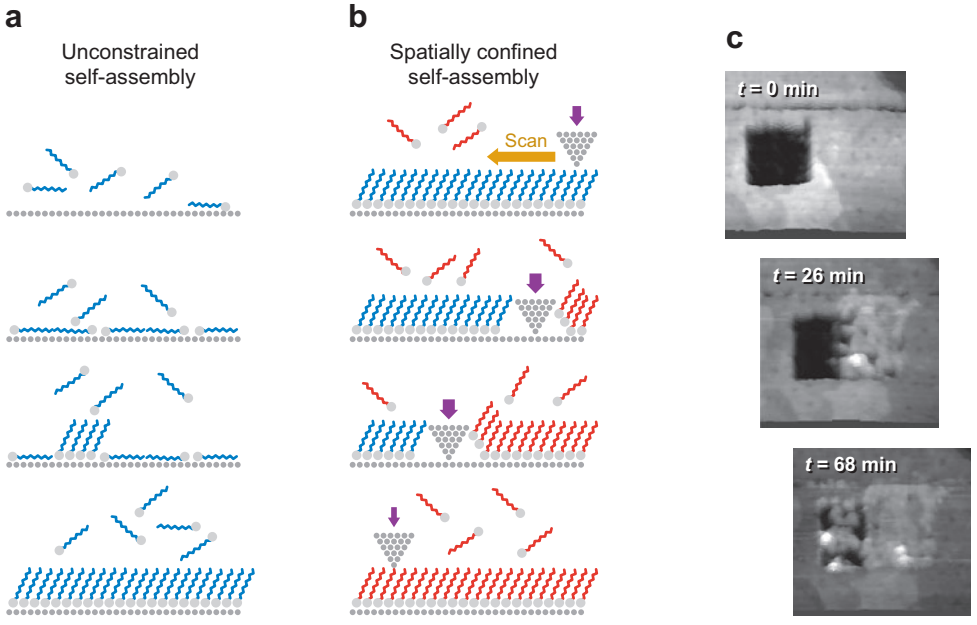

Figure 7

Schematic diagram illustrating the two surface reaction pathways of thiol self-assembly on gold: (*a*) unconstrained in natural growth and (*b*) spatially confined self-assembly in nanografting. (*c*) Side-by-side comparison of C_{18} self-assembly during natural growth onto bare gold (*dark regions*) and nanografting (*rectangular region on the right*). Under identical reaction conditions, self-assembly occurs much faster during nanografting than in natural growth. The scanning size of all images is 150 nm × 150 nm.

the reaction kinetics follows the Langmuir (50, 51) or modified Langmuir (52, 53) relationship, until the coverage reaches ~20%.

Nanografting alters the reaction pathways and kinetics (28). As shown in **Figure 7*b***, the atomic force microscope tip displaces the thiols in the matrix, thus producing a transient reaction environment in which the newly exposed gold surface (i.e., the reactant) is spatially confined by surrounding thiols and the atomic force microscope tip. Such spatial confinement hinders the formation of a lying-down configuration for adsorbing thiols but favors their direct adoption of the standing-up configuration. Therefore, the adsorption follows a new pathway that bypasses the lying-down to standing-up transition (**Figure 7*b***). The new reaction pathway also leads to at least two orders of magnitude faster kinetics (28). The standing-up configuration facilitates the chemisorption of sulfur to gold and the packing of the chains to form the SAM. In addition, the standing-up configuration is also enthalpically favorable because the interactions between the newly adsorbed molecules and the surrounding thiols help stabilize the transition states for the self-assembly process. Thus, the activation energy for the spatially confined self-assembly is lower than that in the unconstrained reaction process.

In natural growth, mixed SAMs form following a similar pathway as illustrated in **Figure 7*a***, and their structures exhibit phase-segregated domains of the components (54–66). In principle, thermodynamic-driven structures (e.g., dominated by large domains of long chains) are expected at low concentrations of reactant, long-reaction times, and with thermal annealing. Conversely, kinetic-driven SAMs (e.g., close to a molecular-level mixing) are favored under high thiol concentration, short reaction times, and low temperatures. The reality lies between the two extremes; in other words, segregated domains would form, whose local structure is the result of the interplay between reaction kinetics and thermodynamics (16, 67).

Owing to the difference in reaction pathways, the nanografting of mixed thiols yields revealing structures (16). **Figure 8** provides unambiguous proof, in which areas of nanografted SAMs and natural grown layers were produced on the same gold surface from the same mixed thiol solution: a 2-μM thiol in 2-butanol with C_{18}/C_{10} = 3:5. **Figure 8*b*** reveals the overall morphology, in which the boundaries of the nanografted area are clearly visible owing to their difference in local structure. The fabricated binary area appears smoother than that of the matrix SAM, supporting the higher degree of molecular mixing in the nanografted SAMs. The lateral heterogeneity is clearly visualized from high-resolution images (**Figure 8*c*,*d***), in which the segregated C_{18} and C_{10} domains and their spatial distribution are clearly visible. The nanografted SAMs as shown in **Figure 8*d*** exhibit smaller C_{18} domains that are less separated than those in the matrix counterpart (**Figure 8*c***).

The degree of spatial confinement (and thus the reaction pathway and kinetics) may be varied by changing the shaving speed (16). **Figure 9*a*** presents three characteristic speeds. At 500 nm s^{-1}, nanografting in a mixed C_{18} and C_{10} solution (1:5 molar ratio with 0.02-mM concentration) resulted in homogeneous mixing of the two components. The average C_{18} domain size is 2.7 nm with a center-center spacing of 5.5 nm. At 3000 nm s^{-1}, the average domain increased to 5.5 nm with a separation

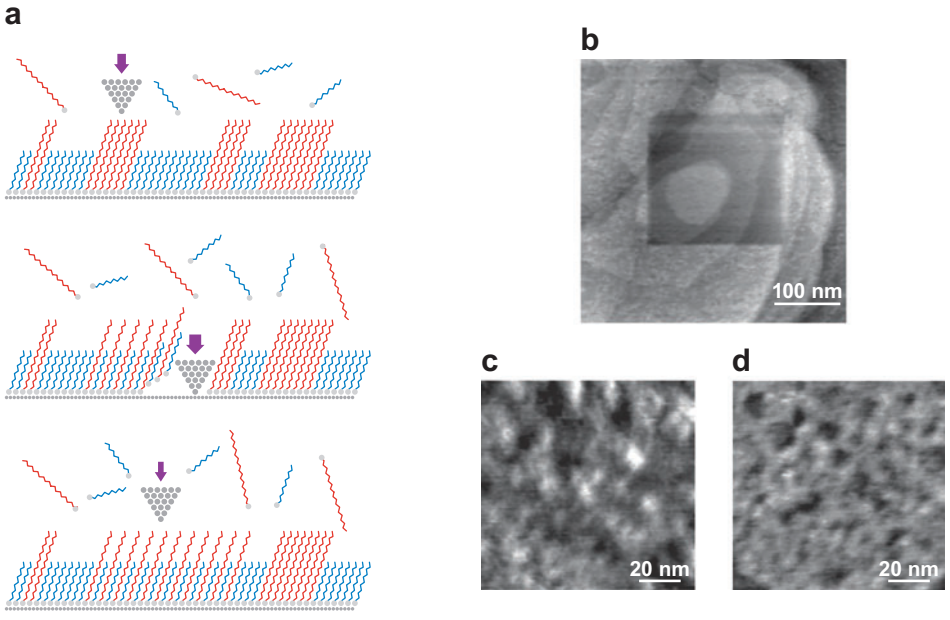

Figure 8

(*a*) Schematic diagram comparing the local domain structures of mixed C_{18} and C_{10} self-assembled monolayers (SAMs) formed in nanografting versus natural growth. (*b*) A 700 nm × 700 nm atomic force microscopy topograph reveals the overall morphology of SAMs produced by the two methods. (*c*) A zoomed-in scan (100 nm × 100 nm) of the matrix SAM. (*d*) A zoomed-in scan (100 nm × 100 nm) in the nanografted area.

of 11.2 nm. At 10,000 nm s^{-1}, the average C_{18} domain increased to 8.9 nm with a 15.0-nm separation, a product nearly the same as that produced via natural self-assembly. To attain larger domains, one can always turn to nanografting single-component thiols with the required functionality (**Figure 9*b***).

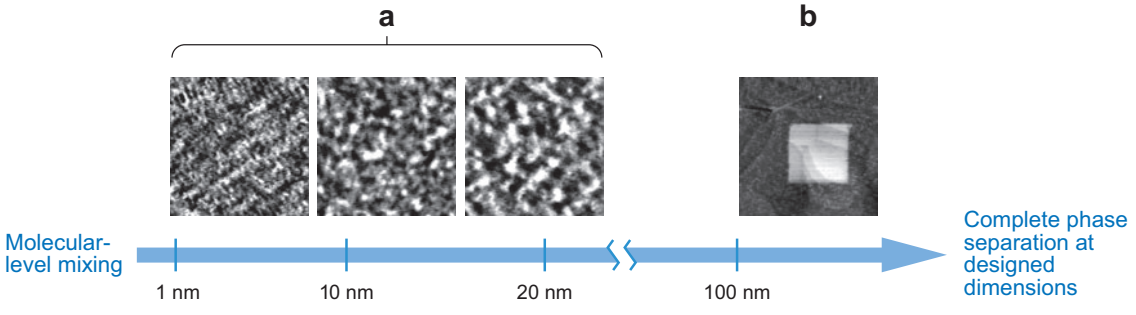

Figure 9

Schematic diagram summarizing the capability of nanografting to regulate local thiol domains, from molecular-level mixing, to nanometer-level domains, to structures with designed geometry and dimension. Imaging size is 100 nm × 100 nm and 400 nm × 400 nm for panels *a* and *b*, respectively.

SUMMARY POINTS

1. Nanografting provides a new and powerful means in surface physical chemistry research.
2. Self-assembled monolayers and multilayers with various chains and termini are characterized by using nanografting to place those unknown molecules into a matrix with known structure or vice versa. The availability of an internal standard in situ allows the unknown structures to be studied and quantified.
3. The same approaches are utilized to determine the density and molecular conformation of DNA on surfaces, as well as the orientation and packing of proteins upon immobilization on surfaces.
4. Nanografting enables systematic investigations of size-dependent mechanics at the nanometer scale (e.g., by producing series of designed nanostructures and measuring their Young's moduli in situ).
5. By precisely engineering ligand nanostructures, researchers can investigate the outcome of biorecognition and protein immobilization reactions to determine the optimal binding of HIV envelope proteins to carbohydrate ligands, the rational design for antibody-antigen recognition, and the local domain structures for protein immobilization.
6. The regulation of the surface reaction mechanism, kinetics, and products is also demonstrated using nanografting by regulating the degree of spatial confinement during the nanoshaving process, which dictates the self-assembly pathway.

DISCLOSURE STATEMENT

The authors are not aware of any biases that might be perceived as affecting the objectivity of this review.

ACKNOWLEDGMENTS

Financial support from the NIH (R21 GM077850-01), NSF (CHE-0244830 and a seed grant from MRSEC-CPIMA), NIST, and the University of California, Davis, is gratefully acknowledged. M. Liu received a graduate fellowship from Tyco Electronics Foundation in Functional Materials while a student at the University of California, Davis. We also thank Z. Deng, Y.H. Tan, and S. Stagner for their assistance in the preparation of this review.

LITERATURE CITED

1. **Xu S, Liu GY. 1997. Nanometer-scale fabrication by simultaneous nanoshaving and molecular self-assembly. *Langmuir* 13:127–29**
2. Tan YH, Liu M, Liu G. 2007. Influence of local ligand structures on biorecognition and protein immobilization. *ACS Nano.* Submitted
3. Amro NA, Xu S, Liu GY. 2000. Patterning surfaces using tip-directed displacement and self-assembly. *Langmuir* 16:3006–9
4. Cruchon-Dupeyrat S, Porthun S, Liu GY. 2001. Nanofabrication using computer-assisted design and automated vector-scanning probe lithography. *Appl. Surf. Sci.* 175:636–42
5. Lee MV, Hoffman MT, Barnett K, Geiss JM, Smentkowski VS, et al. 2006. Chemomechanical nanolithography: nanografting on silicon and factors impacting linewidth. *J. Nanosci. Nanotechnol.* 6:1639–43
6. Liang J, Scoles G. 2007. Nanografting of alkanethiols by tapping mode atomic force microscopy. *Langmuir* 23:6142–47
7. Gorman CB, Carroll RL, He YF, Tian F, Fuierer R. 2000. Chemically well-defined lithography using self-assembled monolayers and scanning tunneling microscopy in nonpolar organothiol solutions. *Langmuir* 16:6312–16
8. Tseng AA, Notargiacomo A, Chen TP. 2005. Nanofabrication by scanning probe microscope lithography: a review. *J. Vacuum Sci. Technol. B* 23:877–94
9. Kolb DM, Simeone FC. 2005. Nanostructure formation at tile solid/liquid interface. *Curr. Opin. Solid State Mater. Sci.* 9:91–97
10. Sugimura H. 2005. Nanoscopic surface architecture based on molecular self-assembly and scanning probe lithography. *Int. J. Nanotechnol.* 2:314–47
11. Piner RD, Zhu J, Xu F, Hong SH, Mirkin CA. 1999. Dip-pen nanolithography. *Science* 283:661–63
12. Salaita K, Wang YH, Mirkin CA. 2007. Applications of dip-pen nanolithography. *Nat. Nanotechnol.* 2:145–55
13. Garcia R, Martinez RV, Martinez J. 2005. Nano-chemistry and scanning probe nanolithographies. *Chem. Soc. Rev.* 35:29–38
14. Liu JF, Von Ehr JR, Baur C, Stallcup R, Randall J, Bray K. 2004. Fabrication of high-density nanostructures with an atomic force microscope. *Appl. Phys. Lett.* 84:1359–61
15. Xie XN, Chung HJ, Sow CH, Wee ATS. 2006. Nanoscale materials patterning and engineering by atomic force microscopy nanolithography. *Mater. Sci. Eng. R* 54:1–48
16. **Yu JJ, Tan YH, Li X, Kuo PK, Liu GY. 2006. A nanoengineering approach to regulate the lateral heterogeneity of self-assembled monolayers. *J. Am. Chem. Soc.* 128:11574–81**
17. Hacker CA, Batteas JD, Garno JC, Marquez M, Richter CA, et al. 2004. Structural and chemical characterization of monofluoro-substituted oligo(phenyleneethynylene) thiolate self-assembled monolayers on gold. *Langmuir* 20:6195–205
18. **Liu GY, Amro NA. 2002. Positioning protein molecules on surfaces: a nanoengineering approach to supramolecular chemistry. *Proc. Natl. Acad. Sci. USA* 99:5165–70**

1. First report on nanografting, which describes the principal, basic procedure and addresses the issue of spatial resolution.

16. Demonstrates that nanografting can regulate the reaction mechanism and products for the self-assembly of mixed SAMs.

18. Presents applications of nanografting in surface biochemistry, especially protein immobilization.

19. Price WJ, Kuo PK, Lee TR, Colorado R, Ying ZC, Liu GY. 2005. Probing the local structure and mechanical response of nanostructures using force modulation and nanofabrication. *Langmuir* 21:8422–28
20. Yu JJ, Nolting B, Tan YH, Li X, Gervay-Hague J, Liu GY. 2006. Polyvalent interactions of HIV-gp120 protein and nanostructures of carbohydrate ligands. *Nanobiotechnology* 1:201–10
21. Liu JF, Cruchon-Dupeyrat S, Garno JC, Frommer J, Liu GY. 2002. Three-dimensional nanostructure construction via nanografting: positive and negative pattern transfer. *Nano Lett.* 2:937–40
22. Zhou D, Wang X, Birch L, Rayment T, Abell C. 2003. AFM study on protein immobilization on charged surfaces at the nanoscale: toward the fabrication of three-dimensional protein nanostructures. *Langmuir* 19:10557–62
23. Garno JC, Yang YY, Amro NA, Cruchon-Dupeyrat S, Chen SW, Liu GY. 2003. Precise positioning of nanoparticles on surfaces using scanning probe lithography. *Nano Lett.* 3:389–95
24. Garno JC, Zangmeister CD, Batteas JD. 2007. Directed electroless growth of metal nanostructures on patterned self-assembled monolayers. *Langmuir* 23:7874–79
25. Liu MZ, Amro NA, Chow CS, Liu GY. 2002. Production of nanostructures of DNA on surfaces. *Nano Lett.* 2:863–67
26. Schwartz PV. 2001. Meniscus force nanografting: nanoscopic patterning of DNA. *Langmuir* 17:5971–77
27. Kenseth JR, Harnisch JA, Jones VW, Porter MD. 2001. Investigation of approaches for the fabrication of protein patterns by scanning probe lithography. *Langmuir* 17:4105–12
28. Xu S, Laibinis PE, Liu GY. 1998. Accelerating the kinetics of thiol self-assembly on gold: a spatial confinement effect. *J. Am. Chem. Soc.* 120:9356–61
29. Liu GY, Xu S, Qian YL. 2000. Nanofabrication of self-assembled monolayers using scanning probe lithography. *Acc. Chem. Res.* 33:457–66
30. Thordarson P, Atkin R, Kalle WHJ, Warr GG, Braet F. 2006. Developments in using scanning probe microscopy to study molecules on surfaces: from thin films and single-molecule conductivity to drug-living cell interactions. *Aust. J. Chem.* 59:359–75
31. Vancso GJ, Hillborg H, Schonherr H. 2005. Chemical composition of polymer surfaces imaged by atomic force microscopy and complementary approaches. *Adv. Polym. Sci.* 182:55–129
32. Wright CJ, Armstrong I. 2006. The application of atomic force microscopy force measurements to the characterisation of microbial surfaces. *Surf. Interface Anal.* 38:1419–28
33. Poirier GE, Pylant ED. 1996. The self-assembly mechanism of alkanethiols on Au(111). *Science* 272:1145–48
34. Poirier GE. 1997. Characterization of organosulfur molecular monolayers on Au(111) using scanning tunneling microscopy. *Chem. Rev.* 97:1117–27

22. Discusses the construction of controllable three-dimensional nanostructures of biomolecules using nanografting, electrostatic immobilization, and specific protein-protein interaction under different buffer environments.

28. First report that nanografting changes the self-assembly pathway and kinetics.

35. Yang G. 2003. *Molecular-level investigations of module membrane systems: scanning tunneling microscopy a nanoengineering approach*. PhD thesis. Univ. Calif., Davis. 168 pp.

36. Engineered a metaloprotein incorporating C-terminal thiol groups to orient and align within a confined alkanethiol matrix on gold using nanografting.

36. Case MA, McLendon GL, Hu Y, Vanderlick TK, Scoles G. 2003. Using nanografting to achieve directed assembly of de novo designed metalloproteins on gold. *Nano Lett.* 3:425–29

37. Brower TL, Garno JC, Ulman A, Liu GY, Yan C, et al. 2002. Self-assembled multilayers of 4,4′-dimercaptobiphenyl formed by Cu(II)-catalyzed oxidation. *Langmuir* 18:6207–16

38. Reveals through experimental and theoretical results the mechanical stabilization of model membrane in aqueous solvent and its disruption in organic solvent.

38. Castronovo M, Bano F, Raugei S, Scaini D, Dell'Angela M, et al. 2007. Mechanical stabilization effect of water on a membrane-like system. *J. Am. Chem. Soc.* 129:2636–41

39. Tambe NS, Bhushan B. 2005. Nanoscale friction mapping. *Appl. Phys. Lett.* 86:1931021–23

40. Gruen DM. 1999. Nanocrystalline diamond films. *Annu. Rev. Mater. Sci.* 29:211–59

41. Krauss AR, Auciello O, Guruen DM, Jayatissa A, Sumant A, et al. 2001. Ultrananocrystalline diamond thin films for MEMS and moving mechanical assembly devices. *Diam. Relat. Mater.* 10:1952–61

42. Jourdan JS, Cruchon-Dupeyrat SJ, Huan Y, Kuo PK, Liu GY. 1999. Imaging nanoscopic elasticity of thin film materials by atomic force microscopy: effects of force modulation frequency and amplitude. *Langmuir* 15:6495–504

43. Muraoka M, Arnold W. 2001. A method of evaluating local elasticity and adhesion energy from the nonlinear response of AFM cantilever vibrations. *JSME Int. J. Ser. A* 44:396–405

44. Rabe U, Kopycinska M, Hirsekorn S, Arnold W. 2002. Evaluation of the contact resonance frequencies in atomic force microscopy as a method for surface characterisation (invited). *Ultrasonics* 40:49–54

45. Uses nanografting and force modulation imaging to investigate the size-dependent elasticity at the nanometer scale.

45. Price WJ, Leigh SA, Hsu SM, Patten TE, Liu GY. 2006. Measuring the size dependence of Young's modulus using force modulation atomic force microscopy. *J. Phys. Chem. A* 110:1382–88

46. Brogi A, Presentini R, Solazzo D, Piomboni P, Constantino-Ceccarini E. 1996. Interaction of human immunodeficiency virus type 1 envelope glycoprotein gp120 with a galactoglycerolipid associated with human sperm. *AIDS Res. Hum. Retrovir.* 12:483–89

47. Wyatt R, Kwong PD, Desjardins E, Sweet RW, Robinson J, et al. 1998. The antigenic structure of the HIV gp120 envelope glycoprotein. *Nature* 393:705–11

48. Nuzzo RG, Allara DL. 1983. Adsorption of bifunctional organic disulfides on gold surfaces. *J. Am. Chem. Soc.* 105:4481–83

49. Camillone N, Leung TYB, Schwartz P, Eisenberger P, Scoles G. 1996. Chain length dependence of the striped phases of alkanethiol monolayers self-assembled on Au(111): an atomic beam diffraction study. *Langmuir* 12:2737–46

50. Jung LS, Campbell CT. 2000. Sticking probabilities in adsorption of alkanethiols from liquid ethanol solution onto gold. *J. Phys. Chem. B* 104:11168–78

51. Yang Y, Disselkamp RS, Szanyi J, Peden CHF, Campbell CT, Goodwin JG. 2006. Design and operating characteristics of a transient kinetic analysis catalysis reactor system employing in situ transmission Fourier transform infrared. *Rev. Sci. Instrum.* 77:094104
52. Dannenberger O, Buck M, Grunze M. 1999. Self-assembly of *n*-alkanethiols: a kinetic study by second harmonic generation. *J. Phys. Chem. B* 103:2202–13
53. Wang RY, Himmelhaus M, Fick J, Herrwerth S, Eck W, Grunze M. 2005. Interaction of self-assembled monolayers of oligo(ethylene glycol)-terminated alkanethiols with water studied by vibrational sum-frequency generation. *J. Chem. Phys.* 122:164702
54. Stranick SJ, Atre SV, Parikh AN, Wood MC, Allara DL, et al. 1996. Nanometer-scale phase separation in mixed composition self-assembled monolayers. *Nanotechnology* 7:438–42
55. Hobara D, Ota M, Imabayashi S, Niki K, Kakiuchi T. 1998. Phase separation of binary self-assembled thiol monolayers composed of 1-hexadecanethiol and 3-mercaptopropionic acid on Au(111) studied by scanning tunneling microscopy and cyclic voltammetry. *J. Electroanal. Chem.* 444:113–19
56. Hobara D, Ueda K, Imabayashi S, Yamamoto M, Kakiuchi T. 1999. Phase separation of binary self-assembled thiol monolayers of 2-mercaptoethanesulfonic acid and 1-octadecanethiol on Au(111). *Electrochemistry* 67:1218–20
57. Kakiuchi T, Sato K, Iida M, Hobara D, Imabayashi S, Niki K. 2000. Phase separation of alkanethiol self-assembled monolayers during the replacement of adsorbed thiolates on Au(111) with thiols in solution. *Langmuir* 16:7238–44
58. Chen SF, Li LY, Boozer CL, Jiang SY. 2001. Controlled chemical and structural properties of mixed self-assembled monolayers by coadsorption of symmetric and asymmetric disulfides on Au(111). *J. Phys. Chem. B* 105:2975–80
59. Sawaguchi T, Sato Y, Mizutani F. 2001. In situ STM imaging of individual molecules in two-component self-assembled monolayers of 3-mercaptopropionic acid and 1-decanethiol on Au(111). *J. Electroanal. Chem.* 496:50–60
60. Klein H, Battaglini N, Bellini B, Dumas P. 2002. STM of mixed alkylthiol self-assembled monolayers on Au(111). *Mater. Sci. Eng. C* 19:279–83
61. Bain CD, Whitesides GM. 1989. Formation of monolayers by the coadsorption of thiols on gold: variation in the length of the alkyl chain. *J. Am. Chem. Soc.* 111:7164–75
62. Chen S, Li L, Boozer CL, Jiang S. 2001. Controlled chemical and structural properties of mixed self-assembled monolayers by coadsorption of symmetric and asymmetric disulfides on Au(111). *J. Phys. Chem. B* 105:2975–80
63. Folkers JP, Laibinis PE, Whitesides GM, Deutch J. 1994. Phase behavior of two-component self-assembled monolayers of alkanethiolates on gold. *J. Phys. Chem.* 98:563–71
64. Tamada K, Hara M, Sasabe H, Knoll W. 1997. Surface phase behavior of *n*-alkanethiol self-assembled monolayers adsorbed on Au(111): an atomic force microscope study. *Langmuir* 13:1558–66

65. Chen SF, Li LY, Boozer CL, Jiang SY. 2000. Controlled chemical and structural properties of mixed self-assembled monolayers of alkanethiols on Au(111). *Langmuir* 16:9287–93
66. Li LY, Chen SF, Jiang SY. 2003. Molecular-scale mixed alkanethiol monolayers of different terminal groups on Au(111) by low-current scanning tunneling microscopy. *Langmuir* 19:3266–71
67. Ryu S, Schatz GC. 2006. Nanografting: modeling and simulation. *J. Am. Chem. Soc.* 128:11563–73

Annual Review of
Physical Chemistry

Volume 59, 2008

Contents

Indexes

Errata

An online log of corrections to *Annual Review of Physical Chemistry* articles may be found at http://physchem.annualreviews.org/errata.shtml